Contribution from the Department of Chemistry, University of Massachusetts, Amherst, Massachusetts 01003, and the Department of Physical Chemistry, University of Nijmegen, Toernooiveld, 6525 ED Nijmegen, The Netherlands

Dynamic and Cooperative Jahn–Teller Distortions in Copper Pyridine *N*-Oxide Complexes, $Cu(pyO)_6X_2$ (X = BF_4^-, ClO_4^-, and NO_3^-): Structural and EPR Studies of Pure and Zinc-Doped Systems

J. S. WOOD,* C. P. KEIJZERS, E. DE BOER, and A. BUTTAFAVA[1]

Received October 16, 1979

The hexakis(pyridine *N*-oxide)cuprate ion, $Cu(pyO)_6^{2+}$, doped into the isostructural diamagnetic zinc complex and in undiluted form as its perchlorate, fluoborate, and nitrate salts, has been investigated by EPR, X-ray diffraction, and magnetic susceptibility measurements. The $Cu(pyO)_6^{2+}$ ion is subject to Jahn–Teller distortions. The EPR spectra, measured as function of the temperature, indicate phase transitions to statically distorted structures, the nature of which are dependent on the anion. For the fluoborate complex, the low-temperature phase is based on a cooperative Jahn–Teller ordering of elongated octahedral complexes which is ferrodistortive while two different antiferrodistortive orderings are proposed for the perchlorate and nitrate complexes. One of these gives a low-symmetry arrangement of elongated octahedra (crystal space group $P\bar{1}$), while for the second the trigonal symmetry of the high-temperature phase is retained and a structure of space group $P3_1$ is proposed. These low-temperature structures are in accord with the results of previously published magnetic specific heat measurements. All high-temperature crystalline phases are trigonal, except one modification of the nitrate complex, which is monoclinic and unstable relative to the trigonal phase. The **g** tensor behavior for this form is in accord with an elongated octahedron. The diluted systems give three-ion-per-cell spectra at low temperature (below 40 K), which are in accord with a tetragonally elongated geometry for the isolated $Cu(pyO)_6^{2+}$ cluster, while line-width measurements give a rough estimate of 40 cm^{-1} for the barrier height between the wells in the warped Mexican hat potential energy surface. Analyses of the room-temperature thermal parameters derived from diffraction measurements for all three copper complexes are also in accord with the presence of Jahn–Teller distortions, and comparison with the isostructural zinc complexes gives an estimate of 0.40 Å for the Jahn–Teller radius. Extended Hückel calculations predict the tetragonally elongated geometry to be marginally more stable than the compressed geometry and give values of 2350 cm^{-1} and 0.28 Å for the Jahn–Teller energy and radius, respectively. In addition, they give **g** and **A** tensor magnitudes in reasonable agreement with experiment.

1. Introduction

Jahn–Teller distorted copper(II) complexes have been subject to intensive investigation during the past several years. For octahedral or near-octahedral complexes with six equivalent atoms in the first coordination sphere, dynamical behavior is commonly observed in the EPR spectra at ambient temperature,[2,3] and structure analysis at this temperature often reveals that the copper ion occupies a site of cubic or trigonal symmetry.[4–6] Such structures have been interpreted in terms of either a dynamic model or a superposition of static Jahn–Teller distorted complexes in which the metal ion has a tetragonal geometry. Even when the copper ion resides at a site of lower symmetry, dynamical properties can sometimes still be observed,[7,8] and this has been described as a pseudo-Jahn–Teller effect.[9]

Lowering the temperature of such complexes leads to a freezing out of the dynamical distortions below the Jahn–Teller transition temperature, and in the case of the pure species such a process is accompanied by at least one first-order structural phase transition.[10–12] The nature of the low-temperature structure is strongly dependent on the nature of the cooperative effects in the lattice, dramatic differences in EPR spectra often being associated with small changes in lattice dimensions or subtle changes in the nature of the counterion.[10,12–15] Studies on doped systems on the other hand are not complicated by cooperative effects, and EPR measurements have confirmed the general form of the warped "Mexican hat" potential energy surface with three equivalent minima, established for the coupling of a doublet (E) electronic state with the Jahn–Teller active vibrations of e symmetry including nonlinear terms in the Hamiltonian.[1,16,17] With the exceptions of Cu(II) doped into MgO[18] and $Zn(imidazole)_6Cl_2$,[19] such measurements for diluted high-symmetry octahedral copper complexes yield a three-site spectrum and have indicated that these potential energy minima correspond to tetragonal elongated structures.

Those complexes of copper(II) that have featured prominently in the development and testing of the theoretical models and whose structural and EPR results are pertinent to the subject matter of the present paper include the series $M_2M'Cu(NO_2)_6$ (M = K^+, Rb^+, Cs^+, Tl^+; M′ = Ca^{2+}, Sr^{2+}, Ba^{2+}, Pb^{2+})[4,10,13–15,20,21] and the tris(ethylenediamine) complex

* To whom correspondence should be addressed at the University of Massachusetts.

(1) On leave from the University of Pavia, Pavia, Italy.
(2) (a) Ham, F. S. In "Electron Paramagnetic Resonance"; Geschwind, S., Ed.; Plenum Press: New York, 1972. (b) Bertini, I.; Gatteschi, D.; Scozzafava, A. *Inorg. Chem.* **1977**, *16*, 1973.
(3) Elliott, H.; Hathaway, B. J.; Slade, R. C. *Inorg. Chem.* **1966**, *5*, 669.
(4) Cullen, D. L.; Lingafelter, E. C. *Inorg. Chem.* **1971**, *6*, 1264. Takagi, S.; Joesten, M. D.; Lenhert, P. G. *Acta Crystallogr., Sect. B* **1975**, *B31*, 1968; **1976**, *B32*, 326.
(5) Cullen, D. L.; Lingafelter, E. C. *Inorg. Chem.* **1970**, *9*, 1858.
(6) Joesten, M. D.; Hussain, M. S.; Lenhert, P. G. *Inorg. Chem.* **1970**, *9*, 151.
(7) Getz, D.; Silver, B. L. *J. Chem. Phys.* **1974**, *61*, 638.
(8) Ammeter, J. H.; Bürgi, H. B.; Gamp, E.; Meyer-Sandrin, V.; Jensen, W. P. *Inorg. Chem.* **1979**, *18*, 733.
(9) Bersuker, I. B. *Coord. Chem. Rev.* **1975**, *14*, 357.
(10) Joesten, M. D.; Takagi, S.; Lenhert, P. G. *Inorg. Chem.* **1977**, *16*, 2680. Mullen, D.; Heger, G.; Reinen, D. *Solid State Commun.* **1975**, *17*, 1249.
(11) Bertrand, J. A.; Carpenter, D. A.; Kalyanaraman, A. R. *Inorg. Chim. Acta* **1971**, *5*, 113.
(12) Bertini, I.; Dapporto, P.; Gatteschi, D.; Scozzafava, A. *J. Chem. Soc., Dalton Trans.* **1979**, 1409.
(13) Harrowfield, B. V.; Pilbrow, J. R. *J. Phys. C.* **1973**, *6*, 755. Harrowfield, B. V.; Dempster, A. J.; Freeman, T. E.; Pilbrow, J. R. *Ibid.* **1973**, *6*, 2058.
(14) Takagi, S.; Lenhert, P. G.; Joesten, M. D. *J. Am. Chem. Soc.* **1974**, *96*, 6606.
(15) Reinen, D.; Friebel, C.; Reetz, K. P. *J. Solid State Chem.* **1972**, *4*, 103. Friebel, C. *Z. Anorg. Allg. Chem.* **1975**, *417*, 197.
(16) Sturge, M. D. *Solid State Phys.* **1967**, *20*, 91.
(17) Englman R. "The Jahn–Teller Effect in Molecules and Crystals"; Wiley: New York, 1972.
(18) Coffman, R. E. *J. Chem. Phys.* **1968**, *48*, 609.
(19) Rao, P. S.; Subramanian, S. *J. Magn. Reson.* **1976**, *22*, 191.
(20) Takagi, S.; Joesten, M.; Lenhert, P. G. *Acta Crystallogr., Sect. B* **1976**, *B32*, 2524.

0020-1669/80/1319-2213$01.00/0

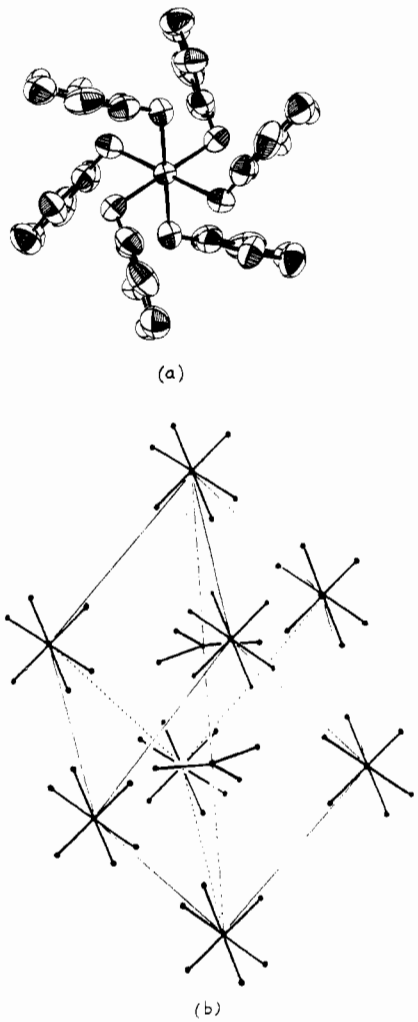

Figure 1. Room-temperature structure of the $M(pyO)_6^{2+}$ complexes: (a) $Cu(pyO)_6^{2+}$ viewed along the crystal threefold axis and (b) a perspective view of the rhombohedral unit cell of $Cu(pyO)_6(NO_3)_2$ showing the packing of cations and anions.

$Cu(en)_3^{2+}$ in the forms of its sulfate and chloride salts.[2,5,12,22] In the case of the hexanitro complexes, the X-ray structures observed below the Jahn–Teller transition temperature are strongly dependent on the nature of the cation, M′, and these differences are also reflected in the EPR spectra.

The series of hexakis(pyridine *N*-oxide)metalate complexes, $M(pyO)_6X_2$, where M = Mn, ..., Zn and X = ClO_4^- and BF_4^-, have proved to be of considerable interest with respect to their electronic properties, since the discovery that they are isostructural and crystallize in the trigonal space group $R\bar{3}$ with one molecule having S_6 symmetry per primitive unit cell.[23-25] The room-temperature structure of the $M(pyO)_6^{2+}$ units and the cation packing are illustrated in Figure 1. As a consequence of the trigonal distortions in their electronic properties and the mode of cation packing in the near cubic primitive unit cell, a variety of magnetic ordering phenomena have been observed at very low temperatures[26] for all the complexes including those of copper which at room temperature have the same trigonal crystal structure as the other cations.[27] However, for the copper complexes, de Jongh and co-workers[28] find that ordering models based on a simple cubic lattice are unsatisfactory, the magnetic behavior of the fluoborate and perchlorate salts being in accord with $S = {}^1/_2$ planar and linear-chain Heisenberg antiferromagnets, respectively. Cooperative phase transitions to different low-temperature structures based on tetragonally distorted Jahn–Teller geometries are therefore suggested by these results, analogous to the situation observed for the hexanitrocuprate complexes with different cations.[10,20]

Table I. Unit Cell Dimensions for $Cu(pyO)_6X_2$ Complexes

anion	temp, K	cell lengths, Å	cell angles, deg	space group
ClO_4	95	$a_R = 9.469$ (3)	$\alpha = 80.9$ (1)	$R\bar{3}$
BF_4	95	$a_R = 9.453$ (3)	$\alpha = 81.3$ (1)	$R\bar{3}$
	20	$a = 9.465$	$\alpha = 81.6$	$P\bar{1}$
		$b = 9.458$	$\beta = 81.6$	
		$c = 9.445$	$\gamma = 81.5$	
NO_3	RT[a]	$a_R = 9.480$ (3)	$\alpha = 83.5$ (1)	$R\bar{3}$
	RT	$a = 9.542$ (4)	$\beta = 100.4$ (2)	$P2_1/c$ ($Z = 2$)
		$b = 9.862$ (4)		
		$c = 18.642$ (7)		

[a] Room temperature.

Simultaneous with these low-temperature magnetic studies we commenced a detailed EPR investigation of both copper complexes and have shown that at room temperature they undergo a dynamic Jahn–Teller effect and that when doped into the isostructural zinc host lattice, the three sites characterized by the tetragonally elongated geometry are produced below ca. 50 K.[29] Further studies demonstrated the importance of the nature of the solvent used for crystallization,[30] and EPR measurements on the pure complexes at low temperatures confirmed that cooperative Jahn–Teller distortions lead to differing structural phase transitions depending on whether the anion is ClO_4^- or BF_4^-.[31] In order to characterize further the influence of the anion on the dynamic to static transition, we have studied the isomorphous nitrate complex, $Cu(pyO)_6(NO_3)_2$, by X-ray diffraction and EPR spectroscopy and have carried out a more detailed study of the low-temperature phases and the influence of the solvent, principally by using EPR spectroscopy. The present paper describes these experimental EPR results, includes an analysis of the thermal motion parameters for the copper complexes derived from the room temperature diffraction results in terms of the Jahn–Teller distortions, and discusses possible structures for the low-temperature phases based on ferro- and antiferrodistortive models. In addition, we have carried out extended Hückel calculations of the Jahn–Teller parameters and the **g** and hyperfine tensors for the $Cu(pyO)_6^{2+}$ species for various degrees of tetragonal distortion.

Simultaneous with our investigations on these systems, we learned of the EPR studies of Professor Reinen at Marburg on the undiluted perchlorate and fluoborate salts. Their results obtained from powder and single-crystal measurements have recently been published.[32]

2. Experimental Section

2.1. Preparation of Complexes. The copper and zinc perchlorate, tetrafluoroborate, and nitrate complexes were prepared according to

(21) Reinen, D. *Solid State Commun.* **1977**, *21*, 137.
(22) Bertini, I.; Gatteschi, D.; Scozzafava, A. *Coord. Chem. Rev.*, in press.
(23) van Ingen Schenau, A. D.; Verschoor, G. C.; Romers, C. *Acta Crystallogr., Sect. B* **1974**, *B30*, 1686. van Ingen Schenau, A. D. Ph.D. Thesis, University of Leiden, 1975.
(24) Taylor, D., private communication, 1974; *Aust. J. Chem.* **1978**, *31*, 713.
(25) Bergendahl, T. J.; Wood, J. S. *Inorg. Chem.* **1975**, *14*, 338.
(26) Algra, H. A.; de Jongh, L. J.; Huiskamp, W. J.; Carlin, R. L. *Physica B+C (Amsterdam)* **1976**, *83B+C*, 71.
(27) O'Connor, C. J.; Sinn, E.; Carlin, R. L. *Inorg. Chem.* **1977**, *16*, 3314.
(28) Algra, H. A.; de Jongh, L. J.; Carlin, R. L. *Physica B+C (Amsterdam)* **1978**, *93B+C*, 24.
(29) de Boer, E.; Keijzers, C. P.; Wood, J. S. *Chem. Phys. Lett.* **1977**, *53*, 489.
(30) Wood, J. S.; de Boer, E.; Keijzers, C. P. *Inorg. Chem.* **1979**, *18*, 904.
(31) de Boer, E.; Keijzers, C. P.; Wood, J. S. *Proc. Int. Conf. Coord. Chem., 19th* **1978**.
(32) Reinen, D.; Krause, S. *Solid State Commun.* **1979**, *29*, 691.

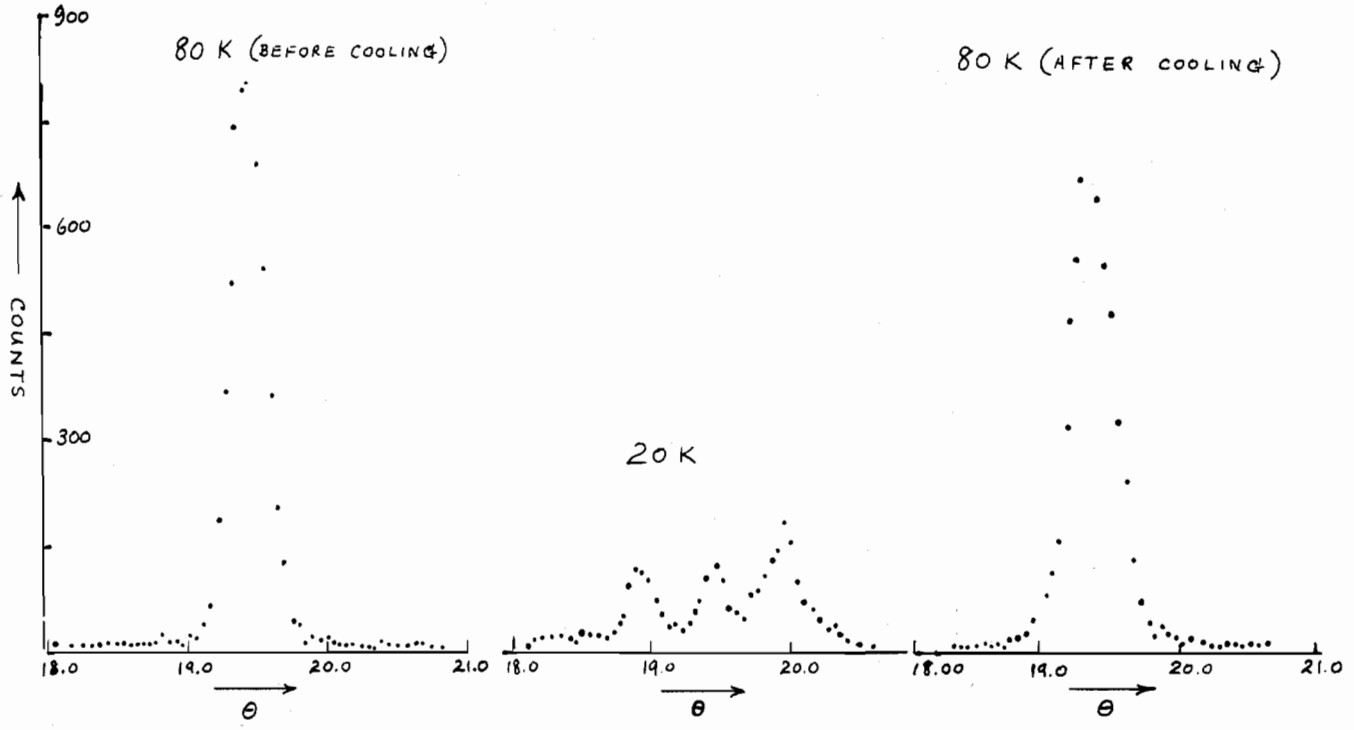

Figure 2. ω scans of the $04\bar{3}$ reflection ($2\theta = 38.9°$) of $Cu(pyO)_6(BF_4)_2$ recorded at 80 and 20 K by using neutron radiation ($\lambda = 1.1621$ Å).

literature methods[33] using ethanol as solvent and an excess of the purified ligand to prevent formation of the four-coordinate complexes. Samples of the isotopically pure ^{63}Cu complexes were prepared from ^{63}CuO. Single crystals of the pure copper complexes and of the copper-doped zinc complexes containing from 0.5 to 5% copper were obtained by slow evaporation of solutions of the complexes in either DMF, ethanol–DMF mixtures, ethanol, or acetonitrile. Ethanol and DMF were the solvents used previously for the preparation of crystals for magnetic specific heat measurements.[27,28] Crystals of the nitrate complex obtained from ethanolic solution were found to be of two types, one having the rhombohedral prism morphology exhibited by crystals of the perchlorate and fluoborate complexes, while the second form had a pronounced acicular habit. Both forms gave satisfactory analyses for $Cu(C_5H_5NO)_6(NO_3)_2$.

2.2. Diffraction Measurements. Various sets of unit cell dimensions for the $Cu(pyO)_6X_2$ complexes are summarized in Table I. The isomorphism of the first form of the nitrate complex with the rhombohedral perchlorate and fluoborate complexes[27] was confirmed by X-ray diffraction and a complete structure analysis carried out at room temperature to obtain the thermal motion parameters.[34,35] Crystals of the second modification were found to belong to the monoclinic system but to convert gradually to the rhombohedral form, a process which is accelerated by grinding. A complete structure analysis of this form was not undertaken. However, the analogous complexes $Cu(CH_3C_5H_4NO)_6^{2+}$ appear to be essentially isomorphous with this monoclinic form, and we have recently found that these contain tetragonally elongated complexes. We conclude therefore that the monoclinic nitrate complex also has the statically distorted geometry.

Cell dimension measurements for the fluoborate and perchlorate salts at 95–105 K indicated that trigonal symmetry was retained for both complexes at this temperature. Measurements at lower temperatures using neutron diffraction have been initiated by Dr. R. K. Brown at Brookhaven National Laboratory, and preliminary results available for the fluoborate complex suggest that a first-order phase transition from the rhombohedral (high-temperature) cell to three triclinic cells occurs close to 60 K. ω scans have shown that strong high-angle reflections are resolved into three components as the temperature is lowered, and an example of such scans for the $04\bar{3}$ reflection is given in Figure 2. The cell dimensions obtained at 20 K show only marginal changes from those at higher temperature. The transition appears to be reversible.

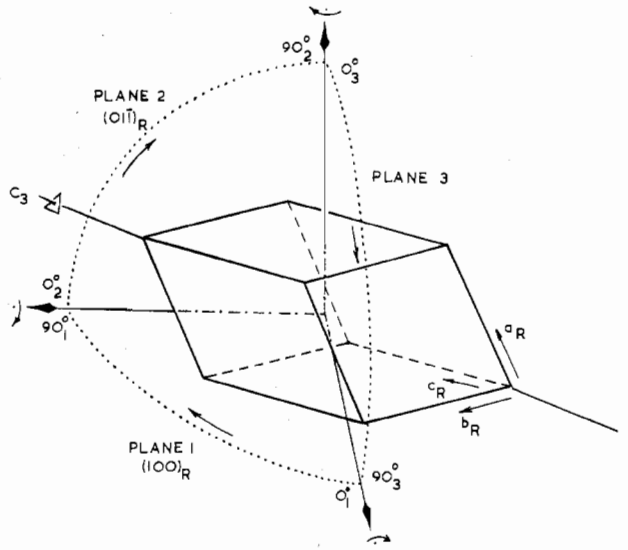

Figure 3. The orientation of the three orthogonal planes in which single-crystal EPR measurements were made for the pure $Cu(pyO)_6X_2$ salts. The origins and directions of rotation conform to those indicated in Figure 5.

2.3. EPR Measurements. Powder measurements were made at room and liquid-nitrogen temperatures on a Varian E-9 EPR spectrometer at X-band (9.5-GHz) frequency equipped with a Varian cryostat. Single-crystal measurements were carried out at both Q-band (35-GHz) and X-band frequencies on a Varian E-12 spectrometer using Oxford Instruments' continuous-flow variable-temperature cryostats, Models BKESR12 (for X-band) and BK35ESR (for Q-band), equipped with temperature controller, Model CE5410. The magnetic fields were measured with a Bruker NMR oscillator, Model B-NM12, and klystron frequencies by a Systron Donner counter, Model 1037-S, and a Hewlett-Packard HP52462 counter, both equipped with plug-in units. Single crystals used for room-temperature measurements at Q-band frequency were aligned by X-ray precession photography, the goniometer with crystal attached being moved to the cavity with an accuracy of ca. 1°. Crystals used for variable-temperature studies were aligned optically by use of polarizing and

(33) Reedijk, J. *Recl. Trav. Chim. Pays-Bas* **1969**, *88*, 499.
(34) Day, R. O.; Wood, J. S. *Acta Crystallogr.*, submitted for publication.
(35) A report of the structure of the corresponding trigonal nickel complex has recently appeared: O'Connor, C. J.; Carlin, R. L.; Filho, A. P.; Joung, K. O. *J. Phys. C* **1979**, *12*, 293.

Table II. Summary of Anion and Solvent Dependence of EPR Spectra of Pure and Zinc-Doped $Cu(pyO)_6X_2$ Complexes

	ClO_4		NO_3	BF_4		NO_3 (monoclinic)
solvent used for crystallization	DMF or DMF/C_2H_5OH	C_2H_5OH, CH_3CN	DMF, C_2H_5OH, CH_3CN	DMF	C_2H_5OH, CH_3CN	C_2H_5OH
A. pure compounds						
1. powder						anisotropy of elongated octahedron; in course of time going over into trigonal modification
JT temp	< 77 K	< 77 K	< 77 K	> 77 K	> 77 K	
above JT temp	apparent isotropic, no hyperfine (as in all spectra of pure compounds)					
below JT temp		anisotropy of compressed octahedron		anisotropy of elongated octahedron		
2. single crystal						1 line at all temperatures; anisotropy of elongated octahedron
JT temp	55 K	60 K	30 K	35 K	42-55 K	
above JT temp	small anisotropy, 1 line					
below JT temp	1 line, small anisotropy	3 lines, of which 2 have ~ equal intensities - anisotropy of compressed octahedron		3 lines of which 2 have equal intensities - anisotropy of elongated octahedron		
	C_2H_5OH, CH_3CN			DMF		
B. doped systems						
1. single crystals				same observations as in crystals from C_2H_5OH or CH_3CN. Besides: varying percentage of molecules with one or two ligands substituted by DMF. These molecules appear in the EPR spectra as statically distorted JT systems at all temperatures with g and hyperfine values slightly different from pure molecules.		
JT temp	similar to: pure compounds from C_2H_5OH					
above JT temp (295 K)	small anisotropy, no hyperfine splitting					
above JT temp (~ 120 K)	small g anisotropy, near-isotropic hyperfine splitting					
below JT temp	3 sites with g and hyperfine anisotropy of elongated octahedron					

conventional microscopes. At X-band frequency, three mutually orthogonal planes of the rhombohedral-shaped crystals were measured with the crystals rotating around $[100]_R$, $[01\bar{1}]_R$, and $[100]_R \times [01\bar{1}]_R$. The crystal planes and rotation directions are indicated in Figure 3.

For Q-band measurements, the crystals were mounted via the $(100)_R$ face, only one crystal mounting being used at this frequency. From such measurements data were available for three sites, so that since the sites in the doped crystals are related by a threefold axis, complete information to determine the **g** and **A** tensors is available. Spectra were recorded at either 5 or 10° intervals, although for regions of overlapping sites, an interval of 1 or 2° was chosen for the doped crystals. The rotation data for the doped crystals were fitted by least-squares procedures using the program SPINHAM,[36] the spin Hamiltonian used being of the form $\mathcal{H}_S = \mu_B \vec{B}\cdot g\cdot\vec{S} + \vec{S}\cdot A\cdot\vec{I} + \vec{I}\cdot P\cdot\vec{I} - \mu_n g_n \vec{B}\cdot\vec{I}$. No restrictions were made with respect to the orientation of the principal axes of the **g**, hyperfine, and quadrupole tensors. The average deviations in the magnetic fields at the least-squares minima were 4.5 and 15 G for the room- and low-temperature data, respectively. For the interpretation of the spectra obtained for the undiluted complexes where no hyperfine structure is observed, the program GAPLSD[36] was used.

2.4. Mass Spectroscopic Measurements. EPR studies suggested that small amounts of solvent of crystallization are present in the crystalline samples used. In order to confirm this observation and to estimate the amounts of solvent present, high-resolution mass spectroscopic measurements were carried out at Delft University of Technology through the cooperation of Dr. J. Reedijk. For the crystals grown from pure DMF or DMF–ethanol mixtures relatively large amounts of DMF, in the range 10–100 ppm on a weight basis, were detected. The upper limit of 100 ppm indicates the presence of 1 molecule of DMF/10^3 molecules of complex. For crystals grown from acetonitrile and ethanol, much smaller amounts of solvent were detected, only in the range 1–10 ppm by weight. For the purposes of the Results and Discussion sections we consider the crystals grown from DMF-containing solutions as solvated and those from ethanol or acetonitrile as unsolvated.

2.5. Magnetic Susceptibility Measurements. These were carried out over a temperature range from room to 2 K on powdered samples of $Cu(pyO)_6(ClO_4)_2$ and $Cu(pyO)_6(BF_4)_2$ on a PARR vibrating sample magnetometer, Model 155. Samples of the perchlorate complex obtained from both DMF and ethanol were measured. Single-crystal magnetic anisotropy measurements were made on the perchlorate salt with a Newport Instruments magnet and cryostat, by using the "angle-flip" technique. Crystals of weight ca. 20 μg were used, and they were mounted on the quartz fiber of the suspension system, parallel to and normal to the trigonal axis of the crystal.

3. Results

3.1. EPR Spectra. 3.1a. Pure Complexes. In this category we include single crystals and powders of the $Cu(pyO)_6X_2$ complexes obtained from ethanol or acetonitrile solution.

Room-temperature measurements of both powder and single-crystal samples of the trigonal complexes yield a single signal, which in the case of the crystals, exhibits a small anisotropy with $g_\perp > g_\parallel$ (parallel to the crystal C_3 axis).

There is no evidence of hyperfine structure in any of the spectra, indicating that spin exchange between adjacent molecules is fast enough to average the hyperfine interactions. There is, however, a variation in the line width in the single-crystal spectra above the Jahn–Teller transition, which ranges from 55 to 100 G, the maximum value coinciding approximately with the direction of maximum anisotropy of the low-temperature **g** tensor. The line widths are reduced somewhat on lowering the temperature, until within 10–15° of the Jahn–Teller transition temperature when appreciable broadening on the signal occurs. The single-crystal EPR spectra of the complexes below the transition temperature will be described separately while a summary of the main results is given in Table II and the principal values of the **g** tensors are listed in Table IIIA.

(36) Keijzers, C. P.; Paulussen, G. F. M.; de Boer, E. *Mol. Phys.* **1975**, *29*, 973.

Table III. Principal Values and Orientations of g, A, and P Tensors Derived from Single-Crystal EPR Measurements

(A) Pure $Cu(pyO)_6X_2$ Complexes

solvent	X	site	g_x	g_y	g_z	T_{measd}, K	T_{JT},[a] K	θ_{C_3}[b]	$\theta_{1,2}$[c]	$\theta_{1,3}$[c]	$\theta_{2,3}$[c]
CH_3CN		1	2.218	2.241	2.075			54.6			
	ClO_4	2	2.219	2.238	2.085	4.2	60 K	53.0	91.7	86.5	84.4
(C_2H_5OH)[d]		3	2.219	2.239	2.082			52.9			
DMF	ClO_4		2.19		2.17	295		0	...	...	...
(DMF/EtOH)			2.192		2.168	4.2		0	...	...	...
DMF		1	2.096	2.092	2.346		35 K (DMF)	59.7			
(C_2H_5OH)	BF_4	2	2.095	2.088	2.341	4.2		56.1	91.6	93.7	94.9
(CH_3CN)		3	2.096	2.086	2.345		48 K (C_2H_5OH)	55.9			
DMF	BF_4		2.19		2.17	295	...	0	...	...	...
DMF (C_2H_5OH)	BF_4	*e*	2.067	2.075	2.367	77	>77 K	...	...	...	...
C_2H_5OH		1	2.221	2.238	2.075			52.4			
	NO_3	2	2.225	2.234	2.082	4.2	30 K	50.6	85.1	85.2	81.0
(DMF)		3	2.223	2.237	2.084			49.8			
C_2H_5OH	NO_3	*f*	2.337	2.088	2.072	295	none	...	...	...	...

(B) Doped $^{63}Cu/Zn(pyO)_6X_2$ Complexes

solvent	X	g_x	g_y	g_z	$10^{-4}A_x$ (P_x), cm^{-1}	$10^{-4}A_y$ (P_y), cm^{-1}	$10^{-4}A_z$ (P_z), cm^{-1}	T_{measd}, K	T_{JT}, K	θ_{C_3}[b]	θ_{C_4}[g]	θ_{g_z,A_z}[i]
CH_3CN (Q-band)	BF_4	2.061	2.088	2.406	−0.1 (−2.9)	0.0 (0.7)	107.7 (2.2)	4.2	47 ↓ 56	57.1	5.8	17.5
DMF/C_2H_5OH (Q-band)	ClO_4	2.187		2.165					47 ↓ 50	0	...	...
		2.074	2.087	2.375[h]	−1.7 (−3.9)	2.3 (1.6)	115.0 (2.3)	295		56.4 50.9	6.2 6.5	5.4
C_2H_5OH (X-band)		2.19		2.17				295	43	0		

[a] T_{JT}, Jahn–Teller transition temperature, corresponds to appearance or disappearance of low-temperature sites. [b] θ_{C_3}: angles (deg) of inclination of principal axes (g_z or A_z) of the g or A tensors with the crystal C_3 axis—values for *g* listed first. [c] θ_{ij}: angles (deg) between principal axes (g_z) of tensors of sites *i* and *j*. [d] Similar behavior also observed for solvents listed in parentheses. [e] Powder measurement. [f] Measurements for triclinic form. [g] Angles (deg) between principal axes of tensors and C_4 axis of elongated octahedron. [h] Results for solvated complex. [i] Degrees.

(i) $Cu(pyO)_6(BF_4)_2$. On cooling of the crystal, the isotropic spectrum is transformed into one giving three magnetically nonequivalent sites, and sample spectra, illustrating the temperature and rotational dependence, are given in Figure 4i. The isotropic and anisotropic signals are present in the spectrum together over a small temperature range. Single-crystal spectra were recorded for the three orthogonal planes indicated in Figure 3. The angular variations of these spectra are illustrated in Figure 5i, and their analysis yielded the **g** tensors for the three sites (Table IIIA). The **g** tensor ($g_\parallel > g_\perp$) is typical for copper(II) in a tetragonally elongated environment.

For each of the low-temperature sites there is a considerable line width variation, and the relative intensities of the three sites differ so as to give two with near equivalent intensity. The intensity of the third site can be either higher or lower and depends on the crystal sample, although in no apparent systematic fashion. This feature is illustrated in Figure 4i,ii where spectra are shown of crystals grown from ethanol and from DMF. In the latter case one site accounts for almost all the spectrum intensity, and we comment on this later. The principal axes of the **g** tensors differ slightly in their inclination to the crystal C_3 axis and in their mutual inclination angles, effects that are presumably related to the crystal phase change and the production of the inequivalent sites or domains (Table IIIA).

In contrast to our results, Reinen and Krause[32] report that they observe the Jahn–Teller transition for single crystals at 90 K. However, magnetic susceptibility and neutron diffraction measurements, together with the EPR spectra depicted in Figure 4i, all support a transition temperature some 40 K lower.

(ii) $Cu(pyO)_6(ClO_4)_2$. As for the fluoborate salt, on cooling of crystals of the perchlorate complex, the nearly isotropic spectrum is transformed into one giving signals for three magnetically inequivalent sites and Figure 4iii depicts this behavior and gives the temperature and rotational dependence. In common with the fluoborate salt the anisotropic and isotropic signals coexist over a small temperature range, the relative intensities of three sites differing, such that two are nearly equivalent, while the third has either higher or lower intensity.

In complete contrast to the former, however, are the **g** tensor relationships for the three sites in the low-temperature spectrum. The three sites have near equivalent tensors but with the reversed *g* relationship $g_\perp > g_\parallel > g_e$. The angular variations of the spectra for the three measured planes are illustrated in Figure 5ii, and this clearly shows behavior which is the reverse of that found for the BF_4^- salt.

(iii) $Cu(pyO)_6(NO_3)_2$—Trigonal Modification. The EPR behavior for single crystals of this form parallels that described above for the crystals of the perchlorate salt; i.e., "reversed" **g** tensors are obtained for the three sites below the transition temperature. The transition temperature is somewhat lower than those for the ClO_4^- or BF_4^- salts.

(iv) $Cu(pyO)_6(NO_3)_2$—Monoclinic Modification. For crystals of this form, only one signal is observed at all temperatures although the nearly isotropic signal characteristic of the high-temperature trigonal form is also very weakly observed in the room-temperature spectra. The exchanged averaged crystal **g** tensor at room temperature exhibits nearly the molecular *g* anisotropy observed for the fluoborate salt, suggesting that the two magnetically inequivalent ions have their tensor axes nearly aligned. We therefore conclude that the statically distorted Jahn–Teller complex having the tetragonally elongated geometry is present in these crystals.

(v) Powder Spectra. The powder spectra and their temperature dependence are illustrated in Figure 6 and are as expected on the basis of the single-crystal spectra, with two

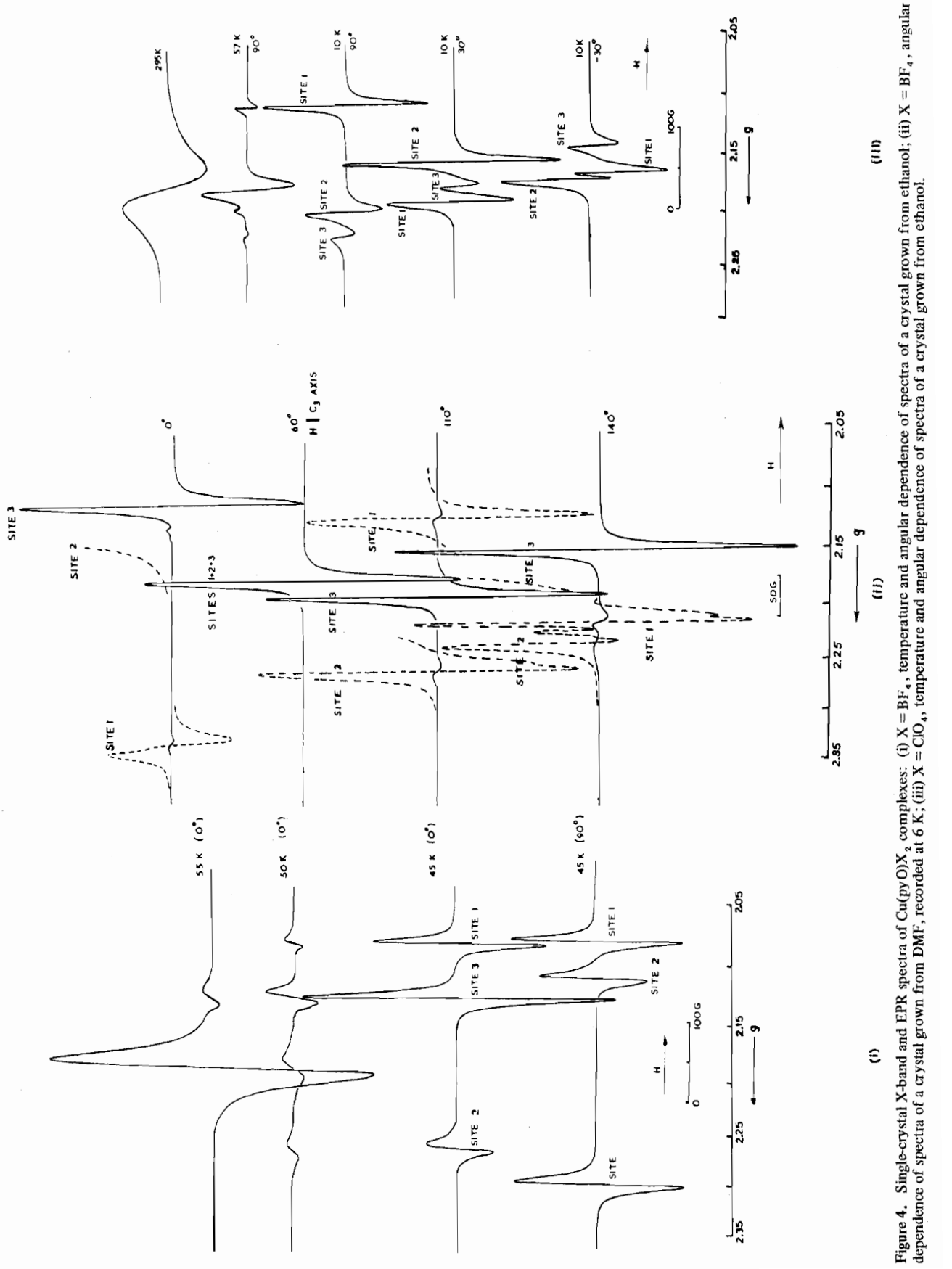

Figure 4. Single-crystal X-band and EPR spectra of $Cu(pyO)X_2$ complexes: (i) $X = BF_4$, temperature and angular dependence of spectra of a crystal grown from ethanol; (ii) $X = BF_4$, angular dependence of spectra of a crystal grown from DMF, recorded at 6 K; (iii) $X = ClO_4$, temperature and angular dependence of spectra of a crystal grown from ethanol.

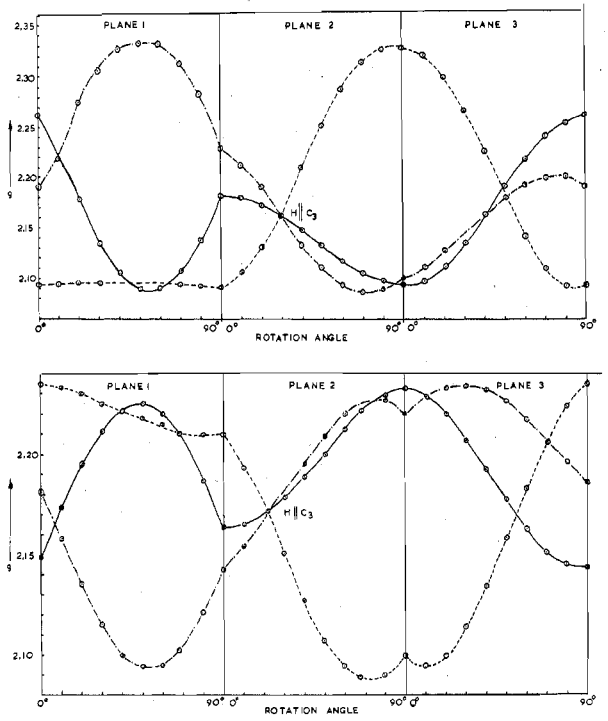

Figure 5. Angular variations of the **g** tensors for three mutually orthogonal planes in single crystals of (i) $Cu(pyO)_6(BF_4)_2$ and (ii) $Cu(pyO)_6(ClO_4)_2$. Ninety degree segments of the planes are illustrated, with the origins and directions of rotation being those indicated in Figure 3.

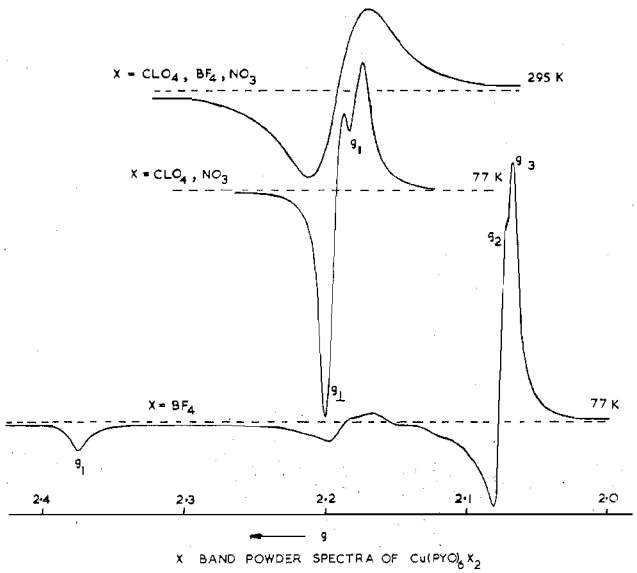

Figure 6. X-band EPR spectra of polycrystalline samples of $Cu(pyO)_6X_2$ complexes.

exceptions: (1) For the fluoborate complex, the Jahn–Teller transition temperature is some 40 K higher than in the single-crystal spectra. The observation concurs with that of Reinen and Krause.[32] (2) The powder spectrum of the monoclinic form of the nitrate complex gives the isotropic signal characteristic of the dynamic $Cu(pyO)_6^{2+}$ complex, in addition to the lines associated with $g_\parallel$ and $g_\perp$ for the single crystal, and after a short interval of time, this signal becomes the predominant feature in the spectrum, suggesting a solid-state phase change from the monoclinic to the trigonal form.

3.1b. Solvated Complexes. Under this heading we describe the results obtained for crystals of the undiluted complexes grown from DMF or DMF–ethanol mixtures.

(i) $Cu(pyO)_6(BF_4)_2$. Crystals of the fluoborate salt give essentially the same EPR spectra as those obtained from ethanol or acetonitrile; i.e., three sites are produced each with $g_\parallel > g_\perp$. For the DMF grown crystals, however, one site or domain predominates and this is evident in the spectra illustrated in Figure 4ii. In addition the transition temperature is significantly lower (Table IIIA).

(ii) $Cu(pyO)_6(ClO_4)_2$. In contrast with the fluoborate salt, the EPR behavior of perchlorate salt crystals grown from DMF differs markedly from that of crystals grown from ethanol. The Jahn–Teller transition is not discernible, there being no change in the spectrum on lowering the temperature from 295 to 4.2 K. As indicated in Table IIIA, an axial **g** tensor ($g_\perp > g_\parallel$) is observed which differs insignificantly from the room-temperature tensor.

(iii) $Cu(pyO)_6(NO_3)_2$. For these crystals, both types of behavior exhibited by the perchlorate salt crystals are found, i.e., that described in 3.1a(ii) and immediately above.

3.1c. Doped Systems. The spectra for the copper complex doped into the zinc host, $Zn(pyO)_6^{2+}$, have been reported previously by O'Connor, Sinn, and Carlin[27] and by ourselves.[29] In addition, the solvents of crystallization have been shown by us to have a profound influence on the spectra.[30] The former authors did not appreciate this point and interpreted their room-temperature spectra for dilute samples grown from DMF solution in terms of a static Jahn–Teller effect for the $Cu(pyO)_6^{2+}$ ion. As well as showing an isotropic signal, these spectra contain two sets of three magnetically nonequivalent sites related by the crystal threefold axis and each having a large *g* anisotropy. Rather than attributing these extra sites to static Jahn–Teller distorted complexes, however, on the basis of our published spectra we believe they arise from solvated complexes.[30] The intensity ratio of the two sets of extra sites is close to 1:6. The **g** and **A** tensors for the stronger set are given in Table IIIB, and they differ only slightly from those of $Cu(pyO)_6^{2+}$ (also reported in Table IIIB) which were derived from low-temperature spectra. The $g_\parallel$ and $A_\parallel$ values for the weaker set are $\sim$2.36 and $\sim 134 \times 10^{-4}$ cm^{-1}, respectively. Due to extensive overlapping of lines in other than the low-field region, it was not possible to obtain the complete tensors for these sites.

The near-zero magnitudes of the perpendicular components of the **A** tensors for both $Cu(pyO)_6^{2+}$ and the stronger set of extra sites made assignment of signals in the high-field regions of the spectra difficult, the forbidden transitions being more intense than allowed ones. Hence the values for A_x and A_y are subject to large uncertainties.

Doped crystals grown for solvents other than DMF are not complicated by the presence of the extra sites and Figure 7 illustrates the behavior of the isotropic signal with temperature for such a crystal containing ClO_4^- as anion at X-band frequency with the magnetic field displaced slightly from the crystal C_3 axis. When the temperature is raised, the signals for the three magnetically inequivalent sites broaden and at ca. 45 K are replaced by the four hyperfine lines of the isotropic spectrum. The widths of the four lines decrease with increasing magnetic field for the temperature range 60–140 K, while above 140 K the spectrum becomes more symmetrical, although the magnitude of the hyperfine splitting is not much affected. Above ca. 190 K all fine structure is absent. In addition to the main signals, a weak isotropic signal also appears at high field in spectra up to ca. 50 K. We presently have no explanation as to its origin.

The resolution of the hyperfine structure of the isotropic signal is at a maximum with the magnetic field parallel to $[111]_R$. The splitting is 35.1×10^{-4} cm^{-1}, very close to the average $(A_x + A_y + A_z)/3$ of the values for the low-temperature sites. The hyperfine lines reach their maximum width

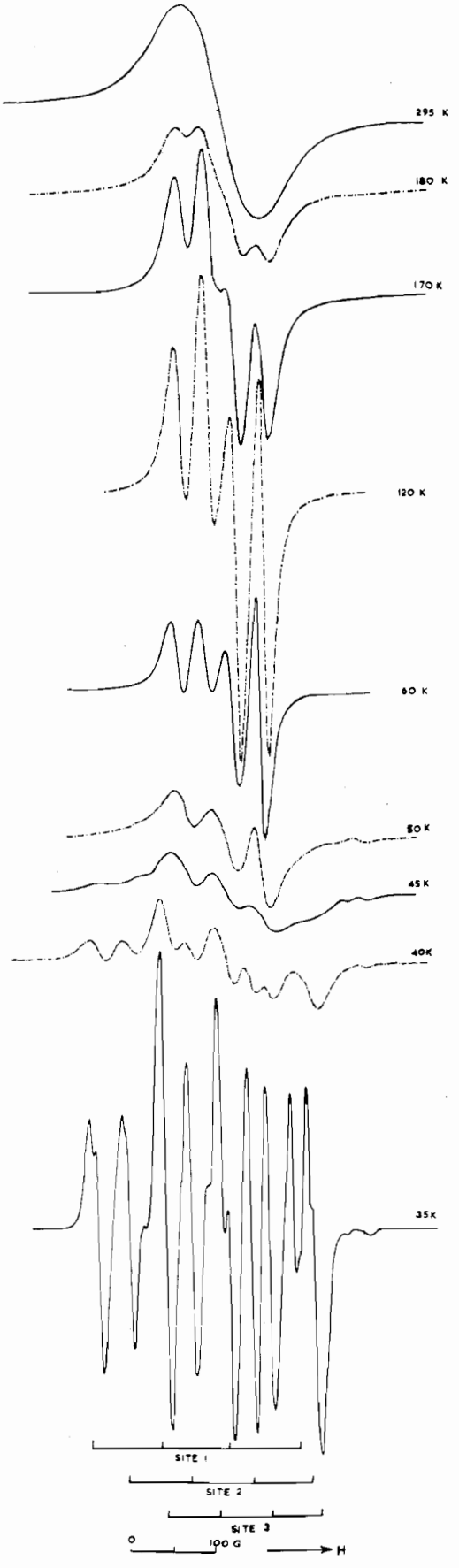

Figure 7. Temperature dependence of the X-band EPR spectra of a single crystal of 0.02 $Cu/Zn(pyO)_6(ClO_4)_2$ obtained from ethanol. The magnetic field is almost parallel to the $[111]_R$ direction.

close to the direction of maximum g anisotropy for the low-temperature sites, an observation which parallels that made for the line width variation of the isotropic signals of the undiluted complexes.

At Q-band frequency the hyperfine structure is not resolved, presumably because of increased line width and consequent overlapping of the signals. In addition, although the low-temperature and isotropic signals coexist over a 10 K range (from 47 to 56 K) for the BF_4^- salt, much as for the undiluted systems, there is a long temperature interval (50–95 K) after the disappearance of the low-temperature signals and before the isotropic signal appears, in the case of the perchlorate salt. The reason for this difference is presently unclear.

The powder spectra which have been recorded by Reedijk and Nieuwenhuijse[37] at temperatures from ambient to liquid nitrogen are in essential agreement with our single crystal results.

3.2. Magnetic Susceptibility Measurements. Bulk susceptibility measurements for the perchlorate and fluoborate salts were made over a temperature range from 2 to 250 K, and we have reported the results in graphical form previously.[30] The susceptibility of both salts may be described by the Curie–Weiss law in two distinct regions: from 55 to 250 K with $\Theta = -21.7$ K for the ClO_4^- salt and -15.2 K for the BF_4^- salt and from 2 to 45 K with Θ values of -2.4 and -2.9 K, respectively, this latter pair of Weiss constants being comparable to those previously reported.[27] There are distinct changes of slope in both plots in the region of 50 K, and these we associate with the first-order phase transition caused by the dynamic to static Jahn–Teller transition. The Θ values are indicative of considerable exchange, the nature of which has been elucidated by specific heat measurements[28] in addition to the low-temperature EPR measurements reported by Reinen and Krause[32] and in the present paper.

The single-crystal susceptibilities, measured for the perchlorate salt over the temperature range 90–295 K, indicate a rather small anisotropy with $\chi_\perp > \chi_\parallel$ in accord with the high-temperature EPR data. The g values derived from these measurements, however, $g_\perp = 2.39$ and $g_\parallel = 2.34$, are higher than those obtained from EPR results.

4. Discussion

The accumulation of EPR results described in the previous section and in earlier reports,[29–32] together with the structural data,[23,27,34] indicate that the $Cu(pyO)_6^{2+}$ ion exhibits a dynamic Jahn–Teller distortion at temperatures above $\sim$50 K and a variety of cooperative effects, based on a statically distorted tetragonal structure, below this temperature. We first discuss the room-temperature X-ray structures of the $Cu(pyO)_6^{2+}$ ions in terms of the dynamic Jahn–Teller effect and then follow this with an analysis of the EPR results. Finally we summarize the results of Hückel calculations of the Jahn–Teller parameters.

4.1. Analysis of Thermal Motions and Comments on Structures. In all the trigonal complexes, the metal ion is crystallographically required to have $\bar{3}$ symmetry with equivalent Cu–O bond distances. Since such symmetry is incompatible with the Jahn–Teller theorem, the complex cation should show a dynamic or disordered static distortion that is incorporated in the thermal motion parameters for the oxygen atoms and possibly the entire ligands. The thermal parameters, given in Table IVA and derived from our own results[34] and those in ref 27, show remarkable similarity for the copper complexes on the one hand and the zinc complexes on the other. The largest root-mean-square displacements of the oxygen thermal ellipsoids respectively make an angle of ca.

(37) Reedijk, J.; Nieuwenhuijse, B., private communication. Nieuwenhuijse, B. Ph.D. Thesis, Twente Technological University, 1974.

Table IV. Thermal Motion Analysis Parameters for $M(pyO)_6X_2$ Complexes

(A) Root-Mean-Square Displacements $U_{ii}^{1/2}$ (Å) for the Metal and Oxygen Atoms and the Angles between the Principal Axes of the Thermal Ellipsoids of the Oxygen Atoms and M–O Bond Vectors (θ_{ii} in deg)

anion	atom	$U_{11}^{1/2}$	θ_{11}	$U_{22}^{1/2}$	θ_{22}	$U_{33}^{1/2}$	θ_{33}
ClO_4	Cu	0.202		0.202		0.171	
	O	0.257	31.4	0.243	58.7	0.209	87.9
BF_4	Cu	0.209		0.209		0.192	
	O	0.270	35.0	0.252	55.0	0.221	88.7
NO_3	Cu	0.202		0.202		0.192	
	O	0.274	36.9	0.252	54.1	0.213	82.6
ClO_4	Zn	0.187		0.187		0.180	
	O	0.234	82.8	0.198	86.4	0.183	8.6
BF_4	Zn	0.208		0.208		0.185	
	O	0.252	88.2	0.219	53.4	0.197	36.6

(B) Rigid-Body Parameters for Pyridine *N*-Oxide Ligands

(i) Amplitudes of Libration (deg) and Angles with the Ligand Inertial Axis System[a]

	x	*y*	*z*
	M = Cu		
L_1 = 7.6 (8.9)[b]	23.5 (33.2)	97.3 (93.3)	67.8 (57.0)
L_2 = 4.7 (4.8)	66.8 (65.3)	81.4 (44.4)	155.1 (124.2)
L_3 = 3.5 (2.5)	93.5 (110.7)	11.3 (45.8)	79.3 (51.6)
	M = Zn		
L_1 = 7.4 (8.5)	34.4 (31.1)	90.4 (90.3)	55.6 (58.9)
L_2 = 4.0 (4.6)	55.6 (59.0)	87.5 (85.6)	143.5 (143.5)
L_3 = 3.3 (3.7)	90.0 (92.3)	2.5 (4.4)	87.5 (86.6)

(ii) Amplitudes of Translation (Å) Reduced to Correspond to Nonintersecting Axis Description and Angles Referred to Ligand System

	x	*y*	*z*
	M = Cu		
T_1 = 0.237 (0.258)	59.8 (58.9)	30.7 (32.6)	85.0 (98.8)
T_2 = 0.202 (0.192)	46.5 (52.3)	108.8 (118.0)	130.5 (129.8)
T_3 = 0.195 (0.214)	58.5 (53.2)	113.3 (103.6)	40.9 (41.2)
	M = Zn		
T_1 = 0.208 (0.219)	47.7 (50.9)	48.0 (48.0)	108.5 (113.2)
T_2 = 0.198 (0.219)	48.5 (48.1)	137.2 (136.4)	99.7 (99.9)
T_3 = 0.166 (0.179)	70.8 (66.7)	96.8 (99.6)	159.5 (154.5)

(iii) Root-Mean-Square Deviation between $(U_{ij})_{obsd}$ and $(U_{ij})_{calcd}$

M	X	rms ΔU_{ij}, Å^2	$\sigma(U_{ij})_{obsd}$
Cu	ClO_4	0.0047	0.0029
Cu	BF_4	0.0068	0.0026
Zn	ClO_4	0.0018	0.0022
Zn	BF_4	0.0021	0.0025

[a] The ligand coordinate system is oriented such that *X* and *Y* lie in the ligand plane with *X* directed along the C_2 axis (O–N bond direction). The origin is taken as the center of mass. [b] The values in parentheses are for the tetrafluoroborate complex.

35° with the Cu–O bonds but are almost orthogonal to the Zn–O bonds, so that in the two zinc complexes, the amplitude of motion along the bond direction is close to the minimum, while in the copper complexes it is near a maximum. Cullen and Lingafelter[5] and more recently Ammeter and co-workers[8] have shown that it is possible to derive information on the magnitude of the Jahn–Teller distortions from the thermal parameter data, and we have followed the approach of the latter in our analysis.

With the assumption that the contributions from the Jahn–Teller inactive vibrations are comparable for the copper and zinc complexes, we compute displacements, $(\overline{\Delta d^2})^{1/2}_{JT}$, for each bond as 0.165 and 0.163 Å, for the perchlorate and fluoborate complexes, respectively. These in turn give values of 0.404 and 0.399 Å for the Jahn–Teller radius, R_{JT}, and these radii lead to predicted Cu–O bond distances of 1.975 and 2.323 Å for the static elongated geometry. Although there are no structural details available for the $Cu(pyO)_6^{2+}$ ion itself in a statically distorted geometry, results are available for the closely related complex $Cu(4\text{-}CH_3C_5H_4NO)_6^{2+}$ formed with the ligand 4-picoline *N*-oxide.[34] This complex, in the form of its perchlorate salt, has Cu–O bond distances of 1.950, 2.032, and 2.386 Å compared to 2.080, 2.115, and 2.176 Å for the Zn–O bonds in the isomorphous zinc complex. These values lead to a Jahn–Teller radius of 0.432 Å for the static geometry.

Turning to the thermal motion patterns for the entire ligands, we have obtained their rigid-body motion parameters by using the generalized *TLS* procedure,[38] and the results are summarized in Table IVB. Comparing the root-mean-square deviations between the observed thermal parameters and those calculated from *T*, *L*, and *S*, with the averaged esd $[\sigma(U_{ij})]$, we find that the ligands behave as essentially independent rigid bodies, this model being somewhat more satisfactory for the zinc than for the copper complexes. The principal difference between the sets of rigid body parameters for the two groups of complexes appears to be in the translational tensors, the magnitudes of the T_1 components being significantly larger for the copper complexes. While we attribute these differences to the presence of Jahn–Teller distortions, we have not attempted to extract any quantitative estimate of R_{JT} from them.

4.2. Analysis of EPR Results. 4.2a. Doped Systems and the Nature of the Static → Dynamic Transition. The results for the doped systems prove that the **g** and **A** tensors for the three low-temperature sites are typical of a copper ion in a tetragonally elongated environment (D_{4h}) with an $|x^2 - y^2\rangle$ ground state and the signal intensities are in accord with equal populations of the three wells in the warped "Mexican hat" potential. There is a small rhombic component to both **g** and **A** tensors, neither of which has its major axis coincident with a Cu–O bond direction of the room-temperature structure. However these results are not unexpected since the distorted complex will only have inversion symmetry.

All the results from EPR measurements are in accord with strong Jahn–Teller coupling in the $Cu(pyO)_6^{2+}$ ion; i.e., E_{JT} (the Jahn–Teller energy) > $\hbar\omega$ (the energy of the active e_g vibration), and indicate that the tunneling splitting 3Γ between the ground-state doublet and the first excited vibronic singlet is very small. However, the fact that the isotropic spectra appear at 45–50 K suggests that the barrier height, *B*, between the potential wells is quite low. Therefore, the overlap between the ground states associated with the different wells may not be negligible, and the tunneling splitting may be comparable with the off-diagonal terms of the Zeeman interaction. This would lead to **g** tensor behavior and relative signal intensities that are quite complex.[39] In such a case, however, Ham[2a,40] has shown how the presence of weak random strain due to crystal imperfections can be expected to dominate other anisotropic effects and lead to a static Jahn–Teller effect when a dynamic effect might have been expected.

In order to assess this possibility, we have calculated an approximate estimate of the barrier height from the temperature variation of the hyperfine line widths in the low-field region of the spectrum. The average lifetime, τ, of the complex in one of the potential wells was derived from the line width with the formula of Hudson,[41] and the resultant plots of ln τ vs. kT^{-1} were approximately linear for the different hyperfine lines, giving values for the barrier height, *B*, of 30–45 cm^{-1}.

(38) Schomaker, V.; Trueblood, K. N. *Acta Crystallogr., Sect. B* **1968**, *B24*, 63.
(39) O'Brien, M. C. M. *Proc. R. Soc. London, Ser. A* **1964**, *281*, 333.
(40) Ham, F. S. *Phys. Rev.* **1968**, *166*, 307.
(41) Hudson, A. *Mol. Phys.* **1966**, *10*, 575.

The applicability of the exponential law $\tau = \tau_0 \exp(B/kT)$ has previously[7] been taken as confirmation that the Orbach[42] process, involving the reorientation to a different well via a vibronic excited state, is the most important in inducing the transition. In this process, however, B is identified as the energy between the ground state and this vibronic excited state rather than being the actual barrier height.

The nature of the transition from the low-temperature anisotropic spectrum to a near isotropic one at higher temperature has been discussed extensively by O'Brien[39] and by Ham,[2a] and the appearance of an isotropic spectrum is consistent with either the presence of excited singlet states which become populated, as described above, or with a motional averaging of the low-temperature spectrum by phonon-induced reorientation of the distorted geometries, the latter being a direct process for which τ varies linearly with T^{-1}.[2a] The **g** and **A** tensors describing the high-temperature spectra are identical for both processes.

While the simultaneous appearance of the anisotropic and isotropic spectra over a small temperature range,[43] together with the temperature dependence of the line widths, may be taken as support for the operation of an Orbach process, the isotropic spectrum illustrated in Figure 7 does not have the symmetrical form expected for an excited vibronic singlet state. The transition temperatures and line widths differ slightly for the different hyperfine lines, indicating a variation in τ values, while the magnitudes of the hyperfine splittings do not follow the axial symmetry of the high-temperature **g** tensor, the best resolved and narrowest spectrum being observed with H parallel to $[111]_R$. These observations are, however, in accord with the expression $\tau << h/(\Delta g \beta H + \Delta A m_I)$ which is the condition for the production of a motionally averaged spectrum. With ΔA negative, the high-field line $m_I = {}^3/_2$ will be the narrowest and have the largest τ value, while for zero Zeeman and hyperfine anisotropies (i.e., H parallel to [111]) the narrowest spectrum will be seen at a temperature which should be somewhat lower than that for the occurrence of motional averaging for any other orientation of the magnetic field.

Finally, we note that the form of the observed spectrum and the m_I line width variation at 60 K is also quite similar to that observed for Cu^{2+}-doped MgO at temperatures above 4 K.[44] For this system however, the low-temperature spectrum (1.2 K) is characteristic of a dynamic Jahn–Teller distortion resulting from zero point motion in the ground state, rather than being a superposition of three axial spectra.[18] Our conclusion therefore is that from the conventional EPR experiments alone it is difficult to decide between alternative transition mechanisms and Ham[2a,40] has shown that in fact strain and relaxation together play a complicated role in determining the nature of the transition.

4.2b. Pure Systems. As indicated in the Results section, the **g** tensors for $Cu(pyO)_6(BF_4)_2$ below the transition temperature and for the monoclinic modification of $Cu(pyO)_6(NO_3)_2$ are in agreement with a tetragonally elongated geometry for the complex ions. The full extent of the g anisotropy is observed in the fluoborate salt, so that the complexes are aligned with their principal axes (long Cu–O bonds) parallel.

The three observed g values for the low-temperature phase of the BF_4^- salt can be attributed to the formation of domains of triclinic symmetry related by the threefold axis of the high-temperature unit cell[45] but between which there is no exchange. The EPR intensities suggest that the relative sizes of these domains can vary between wide limits but that two are equal in size, or nearly so. The neutron diffraction measurements confirm the presence of domains and yield low-temperature unit-cell dimensions that are consistent with one (presumed) centrosymmetric molecule per triclinic cell. The principal axes of the **g** tensors for the three sites are mutually inclined at angles larger than 90° and are inclined to the crystal threefold axis at angles larger than 54.74°. The relative alignment of elongated CuO_6 octahedra for the three sites is then essentially the same as in the doped systems. The proposed structure for one domain, illustrating the ferrodistortive ordering of the elongated octahedra, is given in Figures 8i and 9i. These figures also show the interactions possible between the half-filled $d_{x^2-y^2}$ orbitals on neighboring complex ions that would lead to a magnetic ordering at low temperatures consistent with the observed layer antiferromagnetism.[28]

Although the structure of the monoclinic phase of the nitrate salt has not been determined, we believe it to be very similar to that of the near isomorphous $Cu(CH_3C_5H_4NO)_6$[24] complex, having two tetragonally elongated molecules in space group $P2_1/c$.[34] If this is the case, the close similarity in orientation of the magnetically inequivalent ions (ferrodistortive ordering) would lead to nearly equivalent crystal and molecular **g** tensors, as is observed. The monoclinic cell can then be viewed as the fusion of two rhombohedral cells displaced by half of a lattice translation with respect to each other, and the ease of conversion of this form to the trigonal form is then readily understood.

In contrast to the fluoborate salt, as described earlier crystals of the unsolvated perchlorate salt and of the trigonal modification of the nitrate salt show reversed **g** tensors for the three sites, or domains, with the unique value (assuming axial symmetry) being closely comparable to $g_\perp$ $(=(g_x + g_y)/2)$ for the elongated geometry. Powder measurements at 4.2 K are also in agreement with this conclusion.[32] However, these crystal **g** tensors are not equivalent to the molecular tensors, and although the relation $g_\perp > g_\parallel$ is that expected for a compressed tetragonal geometry, the observed magnitude of $g_\parallel$ is considerably larger than the predicted (near) free-electron value. The tensors are instead in accord with an antiferrodistortive model for which the cooperative Jahn–Teller distortions give a structure having the long axes of the octahedra of alternate molecules mutually orthogonal or nearly so. In the presence of exchange, then, only one axis of the molecular tensor is measured for this model; the other axes corresponding to the average, $(g_\parallel + g_\perp)/2$, of the molecular values. As for the BF_4^- salt the signals for the three noninteracting domains vary in relative intensity, one being weaker than the other two. The crystal tensors for the three domains have a small rhombic component, presumably arising from the small rhombic component in the molecular **g** tensor and the deviations from orthogonality of tensor axes on neighboring molecules. Since the angles of inclination of the axial axes of the tensors for the three domains follow those for the $g_\perp$ components of the sites in the doped crystals, we then conclude that the original molecular tensor axes are approximately oriented along the direction of the rhombohedral cell edges, as appears to be the case for the BF_4^- salt.

The proposed low-temperature structure for one domain, illustrating the antiferrodistortive arrangement of elongated octahedra in the ClO_4^- and NO_3^- salts, is depicted in Figures 8ii and 9ii. Referring to the high-temperature rhombohedral

(42) Orbach, R. *Proc. R. Soc. London, Ser. A* **1961**, *264*, 458.
(43) Borcherts, R. H.; Kanzaki, H.; Abe, H. *Phys. Rev. B: Solid State* **1970**, *2*, 23.
(44) Orton, J. W.; Auzins, P.; Griffiths, J. H. E.; Wertz, J. E. *Proc. Phys. Soc., London* **1961**, *78*, 554.
(45) Loss of the threefold symmetry from $R\bar{3}$ leads to the triclinic space group $P\bar{1}$. However Reinen and Krause[32] discuss the low-temperature structural modifications in terms of pseudotetragonal unit cells, since the high-temperature phase may be considered to be pseudocubic, rather than using triclinic and trigonal symmetries.

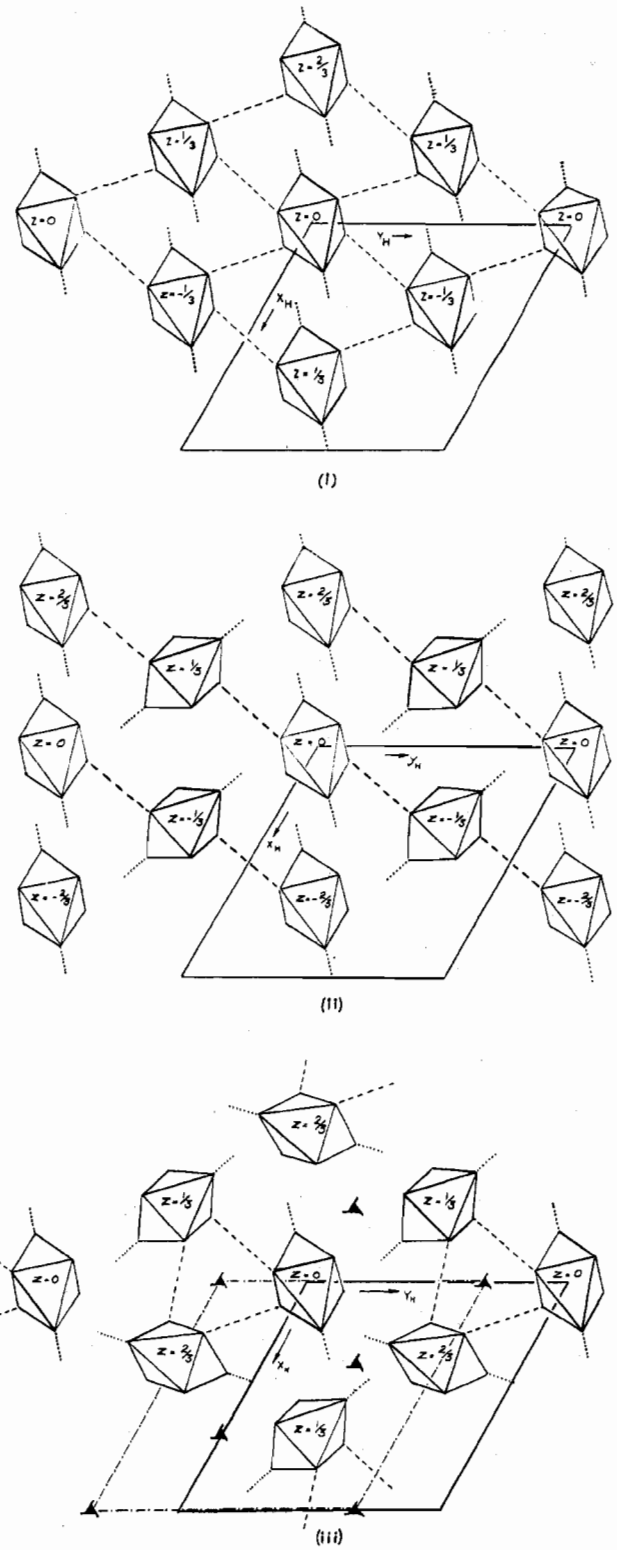

Figure 8. Proposed low-temperature structures of $Cu(pyO)_6X_2$ complexes viewed along the $[111]_R$ direction of the high-temperature unit cell. Broken lines indicate the directions of antiferromagnetic interaction; dotted lines indicate the elongation directions (z axes) of the octahedra: (i) $X = BF_4^-$, ferrodistortive ordering of aligned octahedra leading to planar (two-dimensional) magnetic ordering (crystal system triclinic); (ii) $X = ClO_4^-$ and NO_3^-, antiferrodistortive ordering (alternate layers) of octahedra leading to linear chain (one-dimensional) magnetic ordering (crystal system triclinic); (iii) $X = ClO_4^-$ (DMF grown crystals), antiferrodistortive ordering (spiral chains) of octahedra leading to one-dimensional magnetism (crystal space group $P3_1$).

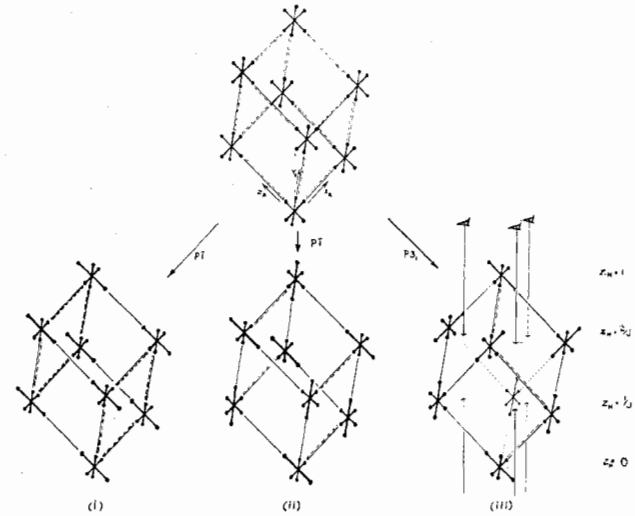

Figure 9. Perspective views of proposed low-temperature structures of $Cu(pyO)_6X_2$ complexes derived from the high-temperature rhombohedral structure and showing in (i) the arrangement for $X = BF_4^-$, all tetragonal axes aligned parallel to z_R, in (ii) the arrangement for $X = ClO_4^-$ and NO_3^-, tetragonal axes aligned alternately parallel to z_R and to y_R, and in (iii) the arrangement for $X = ClO_4^-$ (DMF grown crystals), tetragonal axes aligned alternately parallel to z_R, y_R, and x_R. Resulting 3_1 axes are indicated. Broken lines indicate the directions of the antiferromagnetic interactions.

cell as a basis, this gives an arrangement of elongated octahedra such that alternate layers normal to the $[111]_R$ direction are identical in orientation. In this structure only one-dimensional magnetic ordering, based on the half-filled $d_{x^2-y^2}$ orbitals, would be possible, and de Jongh and co-workers[28] do indeed find that the perchlorate salt behaves as a linear antiferromagnet at very low temperatures, so that this structural model is in accord with both the specific heat and the EPR results. As for the BF_4^- salt, the low-temperature phase should belong to the triclinic system with, in this instance, two molecules per unit cell. Essentially similar conclusions regarding the structures of the low-temperature phases of the unsolvated perchlorate and fluoborate salts were reached by Reinen and Krause on the basis of their EPR results.[45]

4.2c. Solvated Complexes. Crystals of the fluoborate salt grown from DMF give EPR behavior essentially the same as that for the unsolvated crystals except that one domain predominates (Figure 4ii). We thus suggest that the same ferrodistortive model (Figures 8i and 9i) is relevant.

For the crystals of the perchlorate salt obtained from DMF solution, however, the low-temperature crystal **g** tensor has the same axial symmetry as the high-temperature tensor observed for all the salts, with $g_\perp$ slightly larger than $g_\parallel$, but both being comparable to the average of g_x, g_y, and g_z obtained for the doped system. Taking account of the inclination of the principal axis (g_z) to the crystal threefold axis, the relation $g_\perp > g_\parallel$ is thus expected and observed. A structural model, which can be described as being antiferrodistortive and which accounts for the axial symmetry of the crystal **g** tensor and the observed linear antiferromagnetism,[28] is depicted in Figures 8iii and 9iii. Again referring to the parent rhombohedral cell, this proposed structure has an arrangement of elongated octahedra such that their orientations in every third layer normal to $[111]_R$ are identical. Thus the directions of elongation for each layer are successively along x_R, y_R, and z_R, the crystal space group for this proposed arrangement being trigonal $P3_1$, with three molecules per unit cell, which corresponds to the removal of the $\bar{3}$ symmetry element from the room-temperature structure. In this single domain model, the complex ions are only interacting with two neighbors via the half-filled $d_{x^2-y^2}$ orbitals, and one-dimensional antiferromagnetism would again

be expected. Here, however, the pathways for the exchange take the form of spiral chains connecting octahedra related by a 3_1 axis and are orthogonal to one another rather than being collinear.

4.3. Summary of EPR Results. The principal conclusion to emerge from the variable-temperature EPR results described here and the specific heat measurements of de Jongh[28] is that both the nature of the anion and the solvent of crystallization strongly influence the cooperative effects occurring below the Jahn–Teller transition temperature in the undiluted $Cu(pyO)_6^{2+}$ complexes and that the form of the copper complexes in the doped crystals is also affected by the solvent. The behavior we observe for the pure species parallels that found for the $Cu(NO_2)_6^{4-}$ complex;[10,13-15] the change from the ferrodistortive to antiferrodistortive structure in this case being attributed to the change from a "harder" to a more polarizable cation. In the present examples, the anion influence apparently arises from some geometrical feature, although the room-temperature structures are very similar and on the basis of the packing in the lattice (see Figure 1b) it appears the "communication" via the anions, between neighboring cations in adjacent layers of the trigonal cell (i.e., along the rhombohedral edge) should not be significantly different from that between complexes within the same layer. In the fluoborate complex, however, there is a positional disorder of the anion between two orientations, which does not occur for the other two salts. While it is possible that this, together with the differences in mass of the anions, may influence the coupling between complexes in some subtle manner, there is presently no structural evidence that the disorder prevails at lower temperature, closer to the transition point.

The influence of DMF as solvent and the manner in which it affects the coupling in the undiluted complexes is obscure. The mass spectral measurements reveal comparatively little DMF to be present in the solvated crystals, so that the number of substituted complexes produced would hardly seem significant enough to influence the Jahn–Teller cooperative effects. In the case of both BF_4^- and ClO_4^- salts, essentially one domain is formed below the transition temperature, rather than three, with, for the perchlorate salt, accompanying major changes in EPR behavior. Examination of molecular models indicates that solvated complexes $Cu(pyO)_4(DMF)_2^{2+}$ or $Cu(pyO)_5(DMF)^{2+}$ could be readily incorporated into the parent structure with little perturbation to the latter, and from our studies[29,30] on the doped systems we suggest that such species are present in crystals grown from DMF.

4.4. Calculations of the Jahn–Teller Parameters and the g and A Tensors. As described above, the Jahn–Teller radius R_{JT} is calculated to be 0.4 Å. The other parameters needed to describe the warped "Mexican hat" potential energy surface are the Jahn–Teller energy E_{JT} and the barrier height, B, between equivalent minima. An experimental value for E_{JT} of 1510 cm^{-1} is obtained from the lowest energy band in the optical spectra[46] while a rough estimate for B of 30–45 cm^{-1} was obtained from line width measurements of the EPR spectra for the doped systems.

In addition to derivation of the Jahn–Teller parameters from experimental measurements, there have been several reports of calculations of the parameters using both crystal field and molecular orbital models. The former indicates that the compressed geometry is the stable one,[47,48] a result contrary to experimental evidence for nearly all octahedral copper complexes. Simple MO calculations, however, are more in accord with the observed tetragonally elongated geometry.[49-51] We have carried out MO calculations on $Cu(pyO)_6^{2+}$, by using an extended Hückel approach, and the principal results of relevance are given in Table V. Details of the calculational procedure used have been given previously.[52] Calculations were carried out for both tetragonally compressed and elongated geometries (i.e., D_{4h} geometries for the CuO_6 unit) with the displacements of the four equatorial ligands being minus a half of those of the axial ligands. The overall symmetries of the distorted structures are only $C_i(1)$ while for the undistorted structure, the point symmetry is $S_6(3)$. For this geometry, the Hückel calculation yields the one-electron d-orbital sequence $e_g(t_{2g}^{\pm}) < a_g(t_{2g}^{0}) < e_g(e_g)$ (octahedral parentage for a trigonal orientation in parentheses) agreeing with that deduced from an angular overlap approach[53] and with the magnetic properties of various $M(pyO)_6^{2+}$ species.[53-55]

Table V. Calculated and Observed Jahn–Teller and EPR Parameters for $Cu(pyO)_6^{2+}$

parameter[a]	calcd	obsd
R_{JT}, Å	0.28	0.40
E_{JT}, cm^{-1}	2340	1510
B, cm^{-1}	72	30–45
force const, $10^{-5}k$,[b] dyn/cm	1.21	0.46[c]
$\bar{\nu}_{e_g}$, cm^{-1}	147	91[c]
$\bar{\theta}$,[d] rad	0.28	0.25[c]
tunnelling splitting, 3Γ, cm^{-1}	0.036	0.020[c]
cryst field splitting, Δ, cm^{-1}	13 940	8 500
g_x	2.072	2.061
g_y	2.074	2.088
g_z	2.295	2.406
$10^{-4}A_x$, cm^{-1}	48.1	35.9
$10^{-4}A_y$	47.4	35.9
$10^{-4}A_z$	−95.5	−71.8[e]
a_{iso}		−35.9[e]

[a] For the definition of the Jahn–Teller parameters see ref 2a. [b] Calculated as $2E_{JT}/R_{JT}^2$. [c] Values derived from the experimental values of R_{JT}, E_{JT}, and B. [d] Calculated as $(h/2\omega' MT_{JT}^2)^{1/2}$ where M is the ligand mass and ω' is the angular frequency. See ref 16, p 130, and ref 39. [e] Sign from comparison with calculated values.

Ground-state minima occur for axial displacements of ±0.16 Å, and these have total electronic energies (defined as $E_e(Q) = \sum_j n_j \epsilon_j(Q)$ where n_j is the occupation number of the jth MO and ϵ_j its energy) of 0.28 and 0.27 eV for the elongated and compressed geometries, respectively, below that of the octahedron. The small difference of almost 0.01 eV (72 cm^{-1}) between the two geometries represents the barrier separating the minima associated with the elongated structures at 0, $2\pi/3$, and $4\pi/3$ in the "Mexican hat" potential, and the energy 0.28 eV (or 2340 cm^{-1}) is the Jahn–Teller energy for this geometry.

While the computed values of E_{JT} and B represent only a very small fraction of the total electronic energy, they do approximate the values derived from experiment reasonably well and B has the correct sign.

(46) This value for E_{JT} is derived from the lowest energy d–d transition observed at 6050 cm^{-1} in the single-crystal optical spectrum of $Cu/Zn(pyO)_6(ClO_4)_2$ at 77 K and assigned to $^2B_{1g} \rightarrow {}^2A_{1g}$ in D_{4h} symmetry. This contrasts with the value of 7400 cm^{-1} observed in the low-temperature mull spectrum and assigned to this transition by Reinen and Krause.[32] In I symmetry, there are in fact four dipole forbidden transitions expected, all being $^2A_g \rightarrow {}^2A_g$. We are indebted to Dr. Howard Patterson for communicating this result to us.

(47) Ballhausen, C. J.; Liehr, A. D. *Ann. Phys. (N.Y.)* **1958**, *3*, 304.
(48) Fackler, J. P., Jr.; Avdeef, A. *Inorg. Chem.* **1974**, *13*, 1864.
(49) Ballhausen, C. J.; Johansen, H. *Mol. Phys.* **1966**, *10*, 183.
(50) Lohr, L. L., Jr. *Inorg. Chem.* **1967**, *6*, 1890.
(51) Yamatera, H. *Acta Chem. Scand., Ser. A* **1979**, *A33*, 107.
(52) Keijzers, C. P.; deVries, H. J. M.; van der Avoird, A. *Inorg. Chem.* **1972**, *11*, 1338. Keijzers, C. P.; de Boer, E. *Mol. Phys.* **1975**, *29*, 1007.
(53) Wood, J. S.; Bergendahl, T. J. "Abstracts of Papers", 168th National Meeting of the American Chemical Society, Atlantic City, N.J., Sept 1974; American Chemical Society: Washington, D.C., 1976. Mackay, D. J.; Evans, S. V.; McMeeking, R. F. *J. Chem. Soc., Dalton Trans.* **1978**, 160.
(54) Carlin, R. L.; O'Connor, C. J.; Bhatia, S. N. *J. Am. Chem. Soc.* **1976**, *98*, 685.
(55) Carlin, R. L.; O'Connor, C. J.; Bhatia, S. N. *J. Am. Chem. Soc.* **1976**, *98*, 3523.

From the values of the force constant for the Jahn–Teller active vibrations, we compute vibrational energies of 147 (calculated) and 91 (observed) cm^{-1} and zero-point amplitudes of 0.34 and 0.44 Å, respectively, the latter values indicating that the Jahn–Teller distortion in $Cu(pyO)_6^{2+}$ is essentially static in the radial coordinate. However, we find reasonably large zero-point motion in the coordinate θ, assuming that the angular potential can also be treated with a simple harmonic approximation. A value of 16° is obtained for the root-mean-square angular displacement from the set of parameters E_{JT}, R_{JT}, and B.

For appreciable zero-point motion O'Brien[39] has shown that the threefold degeneracy of the ground-state minima is removed and the **g** tensor behavior for the three sites modified. For the Jahn–Teller parameters derived from the Hückel calculation we find that the overlap between the ground-state angular functions in neighboring wells is relatively small and that it yields a value of 0.036 cm^{-1} for the separation of the ground-state doublet and the first excited singlet (3Γ), assuming the calculated barrier height of 72 cm^{-1}. This splitting is comparable to the g anisotropy $(g_{\parallel} - g_{\perp})\beta H$ of 0.038 cm^{-1} for X-band frequency. For localized or static sites to be observed at low temperatures, $\Delta g\beta H$ should, however, be greater than 3Γ. A comparable value for 3Γ is obtained from the experimental values of the Jahn–Teller parameters.

Although a barrier height in the region of 50 cm^{-1} is just consistent with the formation of an anisotropic three-site spectrum at low temperatures, this value is a lower limit. As suggested earlier, random strain is then almost certainly a significant factor in producing the statically distorted sites in this system. The barrier tunneling rate in the lowest vibrational state, calculated according to the formula given by Sturge,[16] supports this picture, for the approximate value of 1.25×10^{10} s^{-1} is in fact appreciably larger than the frequency differences between the three sites.

The **g** and hyperfine tensors were calculated according to the formulas given previously.[52] The elements of the copper atom anisotropic hyperfine tensor were calculated in first order, and contributions from ligand atoms were neglected. The g and A values given in Table V are those for the elongated minimum. The calculated orientations of both the **g** and **A** tensors were found to deviate very little from the molecular axes—taken to be coincident with the M–O bond directions—despite the fact that the complex cation has only $\bar{1}$ symmetry. This is in contrast with the experimental results which, especially for the **A** tensor, show significant deviations from the tetragonal axes.

Acknowledgment. The authors wish to express their thanks to several people who have contributed significantly to this study: Dr. R. K. Brown of Brookhaven National Laboratory for carrying out the low-temperature neutron diffraction measurements; Dr. Jos de Jongh of Kamerlingh Onnes Laboratory, Leiden, for many helpful discussions concerning the low-temperature specific heat measurements; Dr. Jan Noordik for his help with various X-ray measurements; Dr. Jan Reedijk of Delft Technological University, for providing some of the complexes and obtaining the mass spectral data and for his continuing interest and the many helpful discussions that we have enjoyed with him.

In addition, the support of this project by the Scientific Affairs Division of N.A.T.O. through Grant No. 1432 is also gratefully acknowledged.

Registry No. $Cu(pyO)_6(ClO_4)_2$, 14245-15-9; $Cu(pyO)_6(BF_4)_2$, 23013-68-5; $Cu(pyO)_6(NO_3)_2$, 14245-17-1; $Zn(pyO)_6(BF_4)_2$, 23013-69-6; $Zn(pyO)_6(ClO_4)_2$, 23195-17-7.

Contribution from the Departments of Chemistry, University of California, Irvine, California 92717, and Carnegie-Mellon University, Pittsburgh, Pennsylvania 15213

Molecular Orbital Theory of the Properties of Inorganic and Organometallic Compounds. 1. STO-*N*G Basis Sets for Third-Row Main-Group Elements

WILLIAM J. PIETRO,[1a] BEVERLY A. LEVI,[1a] WARREN J. HEHRE,*[1a] and ROBERT F. STEWART[1b]

Received January 22, 1980

An STO-3G basis set has been proposed for the main-group elements of the third row. Equilibrium geometries calculated by using this minimal representation are generally in close accord with available experimental data. The related smaller STO-2G basis set does not perform equally well in the task of structure calculation.

Introduction

The STO-3G minimal basis set[2] has been widely employed for ab initio molecular orbital calculations on polyatomic molecules containing first- and second-row elements. It has met with considerable success in several areas of application, perhaps most dramatically with regard to the calculation of molecular equilibrium geometries. Because of its small size and relatively efficient construction, complete structure optimizations on molecules of moderate size (10–15 atoms) have now become routine. Literally hundreds of theoretical STO-3G equilibrium geometries have appeared in the literature,[3] and the dozens of critical comparisons which have been made with experimentally determined structures indicate an overall high level of performance of the theoretical method.

In this paper we extend the STO-3G basis set to the main-group elements of the third row. Later papers in this series will consider applications to first-row transition metals. We have selected the main-group elements over the metals as a starting point for two principal reasons. For one, there exist a fair amount of gas-phase structural data on molecules containing third-row main-group elements; very little gas-phase data is available for metallic systems. A far more complete assessment of the performance of STO-3G in the former area

(1) (a) University of California. (b) Carnegie-Mellon University.
(2) (a) W. J. Hehre, R. F. Stewart, and J. A. Pople, *J. Chem. Phys.*, **51**, 2657 (1969); (b) W. J. Hehre, R. Ditchfield, R. F. Stewart, and J. A. Pople, *ibid.*, **52**, 2769 (1970).
(3) Compilations include: (a) W. A. Lathan, L. A. Curtiss, W. J. Hehre, J. B. Lisle, and J. A. Pople, *Prog. Phys. Org. Chem.*, **11**, 175 (1974); (b) J. A. Pople, *Mod. Theor. Chem.*, **4**, 1 (1977).

0020-1669/80/1319-2225$01.00/0